AFDEX
Adviser for metal Forming process Design EXpert
Newsletter
Q1 / 2026

MFRC
Metal Forming Research Corporation
www.afdex.com, mfrc@afdex.com
Tel: +82-55-755-7529, Fax: +82-55-761-7529

Contents

1. AFDEX_V24R02 Update and Heat Treatment Module Release

In October 2025, the final update of AFDEX_V24R02 and the Heat Treatment Module were officially released. Since the launch of the new version in June, a series of user-oriented functional enhancements have been implemented. The heat treatment and microstructure analysis module has completed two years of beta testing and is now fully released.

The microstructure prediction program includes capabilities for predicting dynamic recrystallization (DRX), static recrystallization (SRX), and grain growth. The heat treatment program provides new functions covering hardness prediction, annealing, quenching, tempering, and spheroidization. With the release of the latest AFDEX version, users can now perform more comprehensive analyses of both macroscopic and microscopic material characteristics throughout the forming and post-processing stages.

2. AFDEX Simulation Cases

2.1 Anisotropy Modeling

The AFDEX research team has developed an anisotropic elastoplastic finite element analysis program, which was presented at ICPMMT 2025. Figure 2.1 shows the results of an anisotropic elastoplastic finite element analysis of a circular cup deep drawing process using a tetrahedral mesh. The anisotropic elastoplastic analysis capability is scheduled to be available starting from the second quarter of 2026.

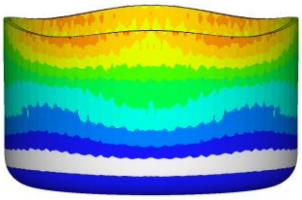

Figure 2.1 Anisotropic elastoplastic finite element analysis using a tetrahedral mesh

2.2 Damage Constant and Critical Damage

The AFDEX research team has developed a practical simultaneous identification method for determining the damage constant and critical damage value based on two experimental tests. This methodology was published in the journal (B. S. Hong et al., Metals 2025, 15, 1376). Figure 2.2 presents a simulation case of the fracture behavior of an energy absorption device. In this example, the Oyane–Okimoto–Shima damage model ($D = \int \left(1 + C\frac{\sigma_m}{\bar{\sigma}}\right) d\bar{\varepsilon}$) was applied, and the damage constant $C = 0.82$ and the critical damage value D=1.29 were identified. When these values are used, the simulation results provide predictions that simultaneously satisfy both the tensile test and the energy absorption test from an engineering standpoint.

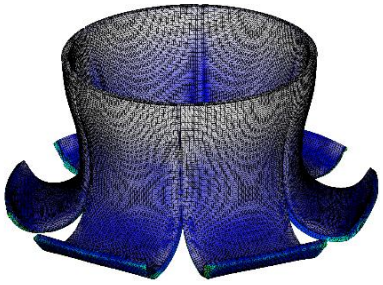

(a) Analysis result of the impact test (Final stage)

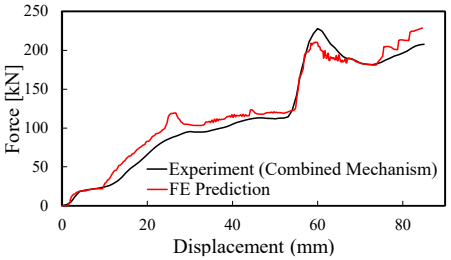

(b) Stroke–impact load curve

Figure 2.2 Impact test simulation of an energy absorption device

2.3 Fillet Rolling: High-accuracy, Cost-efficient Analysis Modeling

In 2025, extensive research was conducted on the analysis techniques for the fillet rolling process of high-performance bolts, leading to the proposal of various simulation models. Approaches such as optimized load application methods and the use of geometric symmetry were introduced to enhance numerical stability and computational efficiency. Figure 2.3(a) shows a full-domain finite element analysis model of the fillet rolling process for a titanium bolt, while Figure 2.3(b) compares the simulation results with experimental measurements. Figure 2.3(c) presents the stress cycles experienced at critical locations during fatigue testing. The results indicate that fillet rolling significantly reduces both the mean value of the maximum principal stress from 730 MPa to 200 MPa and its stress amplitude from 400 MPa to 200 MPa. This reduction leads to a substantial improvement in the fatigue life of the bolt. The major research outcomes were published in J. Manufact. Process. (V. 151, 2025, 490–505) and J. Mater. Res. Technol. (V. 37, 2025, 3788–3800).

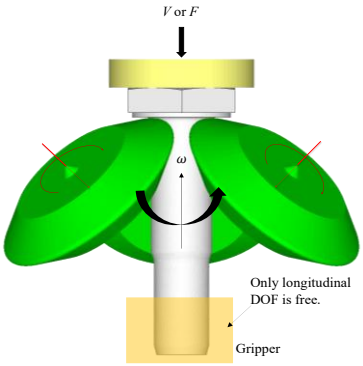

(a) Full-domain analysis model

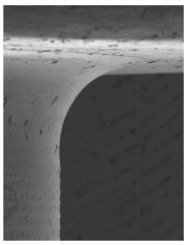

Experiment

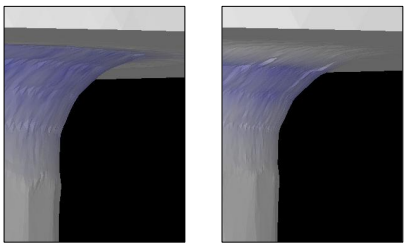

Full analysis model | Practical analysis model

(b) Comparison of experimental results with predictions from the full-domain and practical models

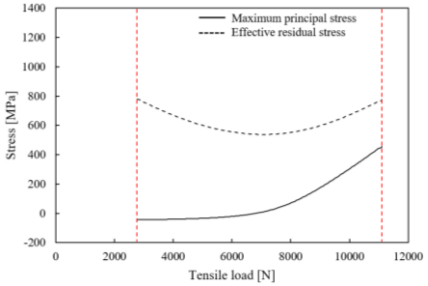

(c) Structural analysis results for fatigue testing (applied load–maximum principal stress and effective residual stress curves)

Figure 2.3 Fillet rolling process analysis

2.4 Flow Curve Identification Using Elastoplastic FEM

AFDEX MAT provides flow curves based on the rigid–plastic finite element method, which can accurately predict tensile tests from an engineering perspective. However, when these flow curves are applied to tensile simulations using the elastoplastic finite element method, noticeable discrepancies from experimental results may occur. Recently, the use of elastoplastic finite element analysis has been increasing, particularly for sheet metal forming and sheet or plate forging simulations, where elastic effects play a critical role.

To address this issue, the AFDEX research team developed a practical flow curve identification method using the elastoplastic finite element method, which improves flow curves originally obtained from rigid–plastic analysis. This approach leverages the key advantage of the rigid–plastic method, namely the stable acquisition of the initial flow curve. Figure 2.4(a) compares flow curves obtained using rigid–plastic and elastoplastic finite element methods. Figure 2.4(b)

compares the tensile test curve predicted using the elastoplastic-based flow curve with experimental results, showing excellent agreement.

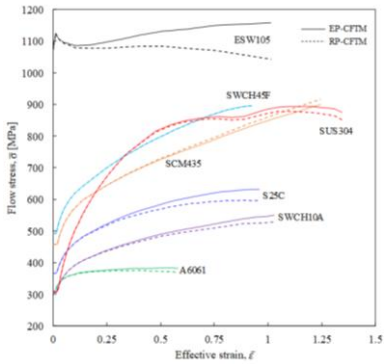

(a) Comparison of flow curves obtained by rigid–plastic and elastoplastic FEM

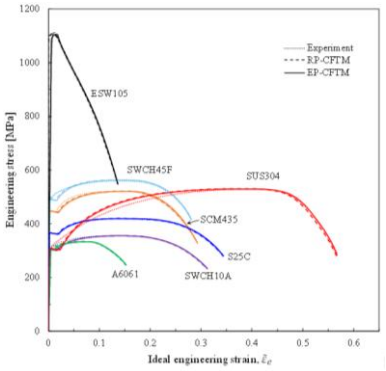

(b) Comparison between elastoplastic FEM predictions and experimental tensile test results

Figure 2.4 Flow curve identification using elastoplastic FEM

2.5 Standard Tensile Properties from Conventional Tensile Tests

Despite standardized tensile testing procedures, two distinct different standards exist, and in practice, these standards are often not strictly followed. As a result, it is difficult to secure consistent and standardized tensile test data, highlighting the need for reliable data normalization and accumulation. To address this issue, an analytical elongation calibration function was developed, and its effectiveness was numerically validated (Kim et al., 2025, Mater. & Des., 113851).

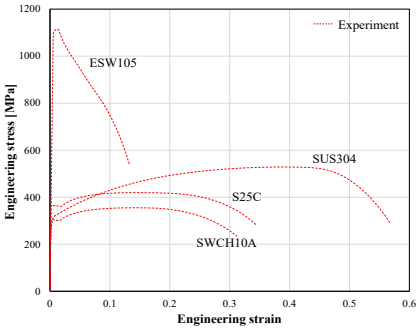

(a) Tensile tests with different GLPD values

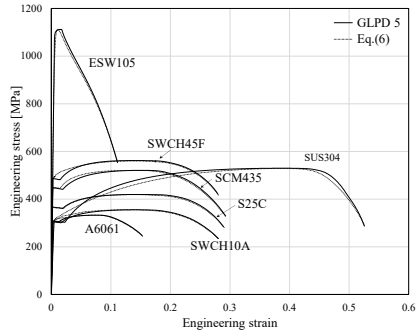

(b) Comparison of numerical and analytical results for standardized tensile tests with GLPD = 5

Figure 2.5 Scientific and data-driven standardization of tensile testing

By applying this elongation calibration function, which acts as a mapping function, nominal stress–strain curves obtained from non-unified tensile specimens with varying gauge length-to-diameter ratios (GLPD, Figure 2.5(a)), as shown in can be converted into a unified standard tensile curve with GLPD = 5 (Figure 2.5(b)). According to the analysis results, the error introduced by this transformation is negligible.

2.6 Flow Curve Identification from Tube Materials

To identify the flow curve of tube materials, several researchers have applied tensile testing on sheet metal or conducted tensile testing on tube using a snug-fitting plug. The AFDEX research team leveraged the high accuracy of the snug-fitting plug approach and developed a flow curve identification method that integrates finite element analysis with tube tensile testing (B. S. Hong et al., Int. J. Adv. Manufact. Technol., V. 141, 2025, 5373–5388). As shown in Figure 2.6(a), the finite element model consists of multiple bodies. An optimal flow curve was obtained by iteratively minimizing the discrepancy between the predicted load–displacement curve, based on the current flow function, and the experimental curve.

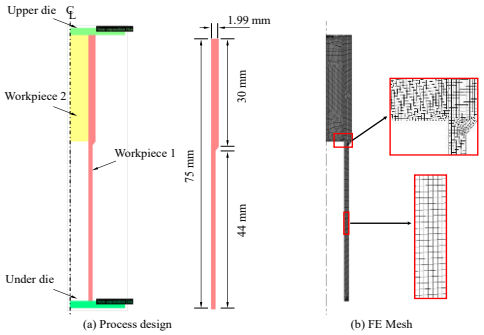

(a) Finite element model for tube tensile testing

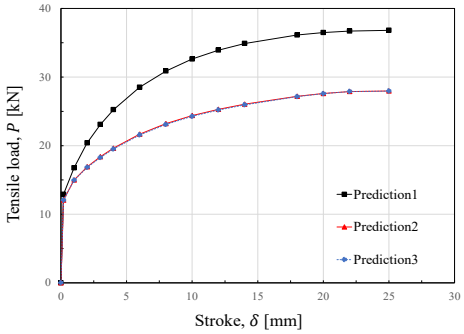

(b) Stroke–load curves of tube tensile tests

Figure 2.6 Flow curve identification for tube materials

Figure 2.6(b) highlights the favorable convergence characteristics of the proposed method. Although the tensile curve predicted using the initially assumed flow curve (Prediction 1) exhibits a large deviation from the experimental curve (identical to Prediction 3), a single iterative update produces a prediction (Prediction 2) that closely approaches the experimental result. After two optimization iterations, the tensile curve predicted using the final flow curve (Prediction 3) agrees with the experimental curve within an error of 0.16%. This material exhibits a high strain-hardening capability, resulting in rapid convergence. For materials with lower strain-hardening behavior, however, a larger number of iterations may be required.

2.7 Flow Curve and Friction

Friction is an inherently complex phenomenon. Most studies on friction consistently emphasize its strong dependence on factors such as contact pressure, temperature, sliding speed, surface expansion ratio, relative velocity, material properties, and lubricant type and condition. Nevertheless, in practical process simulations, many researchers still rely on simplified friction laws using a constant friction coefficient or friction factor. There are two main reasons for this practice. First, forging simulation technologies have traditionally focused on macroscopic phenomena, particularly the final shape of forged products, rather than high-precision analysis or accurate load prediction. Second, the primary target materials have often been steels and other materials with high strain-hardening capacity, in which the influence of friction tends to be secondary.

In particular, many researchers remain dependent on the constant shear friction law. Wilson (W. R. D. Wilson, Friction and lubrication in bulk metal-forming processes, Journal of Applied Metalworking, Vol. 1, 1978, pp. 7–19) offered a critical and somewhat cynical perspective on this tendency, attributing it to shortcomings in early engineering education. He suggested that friction concepts derived from threaded fastener mechanics were inappropriately applied to metal forming problems, despite the fundamentally different nature of friction in these two contexts.

For materials with low strain-hardening capacity, such as aluminum alloys or ESW materials, friction plays a much more dominant role in the forming process. This effect is further amplified when thickness reduction varies spatially or when significant shape changes occur depending on the material flow direction, as in forward–backward extrusion processes.

The selected application case is a forward–backward extrusion process in which achieving the desired deformation shape is particularly challenging. Figure 2.7 presents the friction conditions required to accurately predict the optimal deformation shape shown in Fig. 8. Meaningful shape prediction is not possible when using a constant friction factor or coefficient.

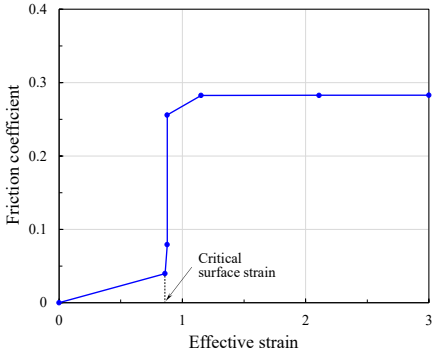

Figure 2.7 Lubrication regime change behavior

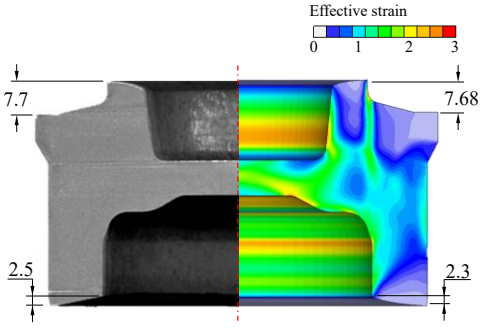

Figure 2.8 Comparison between experimental and simulation results

The friction coefficient function shown in Figure 2.7 exhibits a typical lubrication regime change, in which the friction coefficient increases abruptly once the interfacial material reaches a certain level of strain. This phenomenon is highly likely to occur during cold and hot forging of low strain-hardening materials such as aluminum.

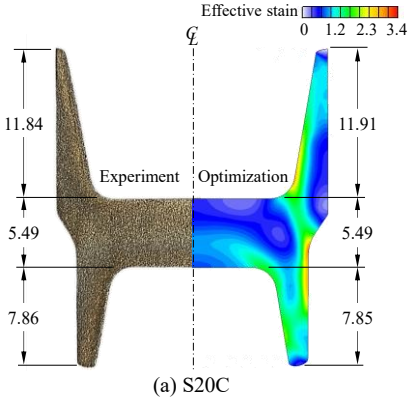

(a) S20C

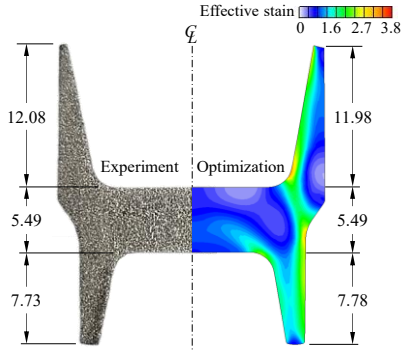

(b) A6061 alloy

Figure 2.9 Cases requiring consideration of lubrication regime change

Figure 2.9 compares simulation and experimental results for forward–backward extrusion processes of steel and aluminum under identical conditions except for the friction conditions. Notably, the predictions were obtained using the optimized friction coefficient function of effective strain exhibiting the lubrication regime change. The simulations using various conventional friction coefficients demonstrated that neither the Coulomb friction law nor the constant shear friction law can reproduce the experimental outcomes. In other words, predictions based on conventional friction laws show clear discrepancies from experimental results, particularly in terms of final shape.

2.8 Flow Behavior of Carbon Steel at Room Temperature

Among carbon steels, S10C, S20C, and S45C are widely used for cold forging applications. These three materials were subjected to heat treatment under identical conditions for cold forging, followed by carefully controlled tensile tests conducted by a NADCAP-accredited testing laboratory (Tesco). Figure 2.10(a) shows the tensile test results, while Figure 2.10(b) presents the flow curves obtained using AFDEX MAT. For this purpose, a generalized Hollomon model was adopted, in which the strength coefficient is treated as a function of effective strain, referred to as a strength coefficient function.

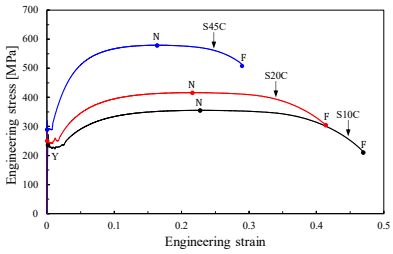

(a) Tensile test results of representative carbon steels

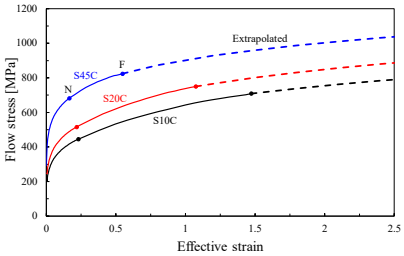

(b) Flow curves

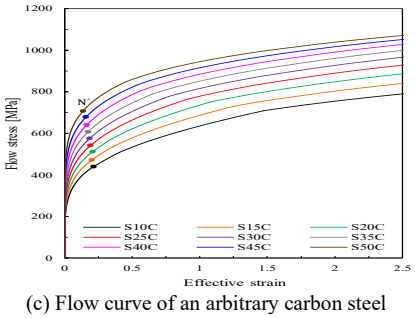

(c) Flow curve of an arbitrary carbon steel

Figure 2.10 Tensile test results and flow curves of carbon steels

The analysis revealed that the key flow behavior parameters can be expressed as functions of carbon content. Based on this observation, the flow function was formulated explicitly as a function of carbon content. As shown in Figure 2.10(c), this formulation enables the derivation of a flow curve for an arbitrary carbon steel composition.

2.9 Multi-Stage Roll Flow Forming

Flow forming, including spinning and roll forming, is a type of incremental metal forming process in which rotating rollers are used to form products of various shapes, such as sheet metals, hollow cylinders, and conical geometries.

In the example process, two additional rollers with different geometries (Roll 2 and Roll 3) were introduced in addition to the initial roller pair (Roll 1-1 and Roll 1-2). The material thickness is progressively reduced through a total of three forming stages. Figure 2.11(a) shows the 360° finite element model used in the analysis.

During the simulation, Roll 1-1 and Roll 1-2 operate simultaneously, followed by sequential forming by Roll 2 and Roll 3. Figure 2.11(b) presents the final simulation result for a virtual automotive wheel flow forming process.

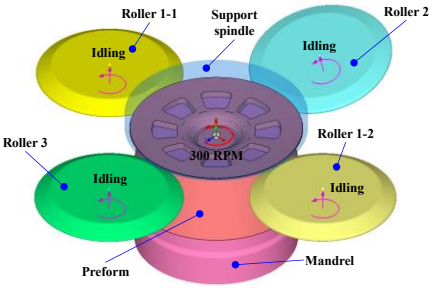

(a) 360° process simulation model

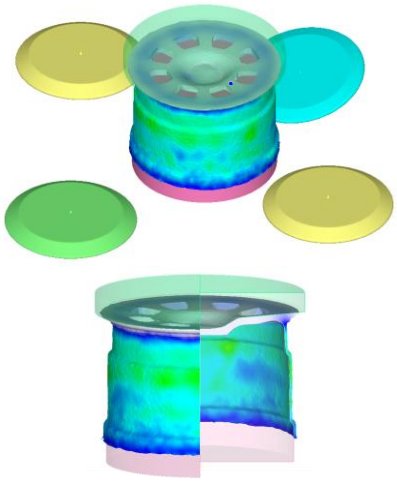

(b) Simulation result

Figure 2.11 Multi-stage flow forming analysis of a virtual automotive wheel

2.10 Enhanced Sheet Metal Forming Analysis

To demonstrate the enhanced sheet metal forming capabilities of AFDEX, a simulation case of a stamping process for a cathode current collector component used in lithium-ion batteries is presented. The material employed was a 2.0 mm-thick aluminum A1050-H18 sheet. The process and die were designed to be compatible with a 250-ton mechanical press and consisted of a total of eight forming stages.

Figure 2.12(a) illustrates the deformation history at each stage, while Figure 2.12(b) compares the predicted shape with the experimental result.

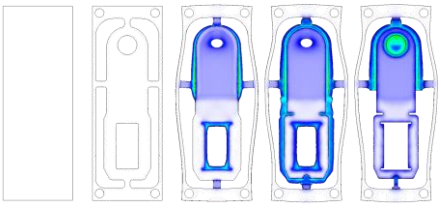

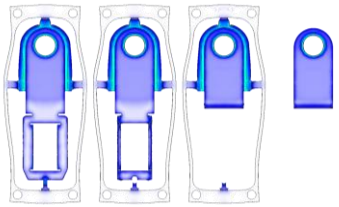

(a) Deformation history from Stage 1 to Stage 8

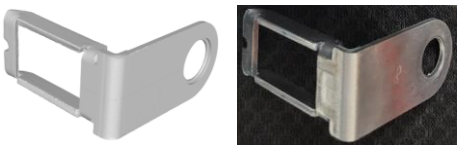

(b) Comparison of simulation and experimental results

Figure 2.12 Sheet metal forming analysis of a current collector component

2.11 Heat Treatment Analysis

Using the AFDEX 2D/3D heat treatment module, major processes such as annealing, quenching (Figure 2.13(a)), tempering, quenching and tempering (QT, Figure 2.13(b)), and spheroidization (Figure 2.13(c)) can be analyzed. Users can define flexible heat treatment cycles by controlling time, temperature, and convective heat transfer coefficients. By selectively activating relevant phenomena, microstructural evolution during each cycle can be accurately tracked. Hardness is calculated based on grain size and phase fraction data using the Hall–Petch relationship.

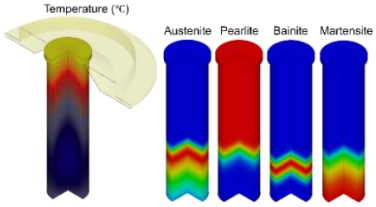

(a) Jominy end-quench test of AISI 52100 according to ASTM A255

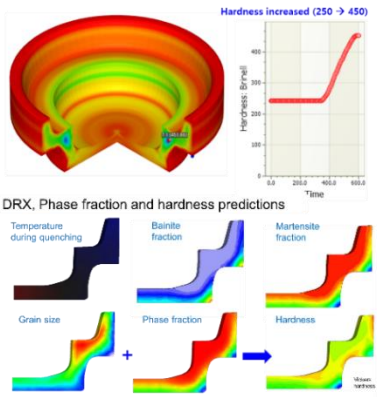

(a) Brinell hardness of a bearing race

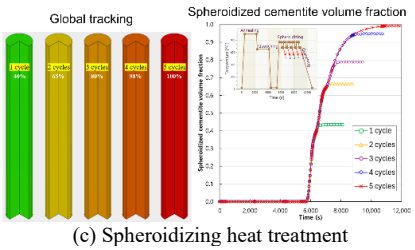

(c) Spheroidizing heat treatment

Figure 2.13 Heat treatment simulations

2.12 Surface Expansion Ratio Visualization

For each location on the material surface, the surface expansion ratio can be visualized in the post-processing module, as shown in Figure 2.14. This parameter is directly related to changes in friction conditions during metal forming and therefore plays a critical role in achieving more realistic friction modeling. In addition, a new friction coefficient function that incorporates a weighting function based on the surface expansion ratio is currently supported.

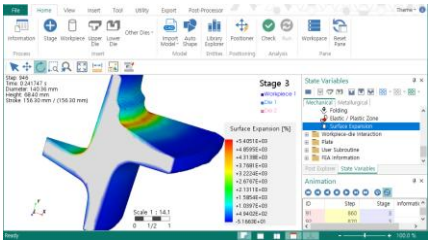

Figure 2.14 Surface expansion ratio visualization in 3D

2.13 Improved Material-to-Material Contact

This section presents application examples of the improved material-to-material contact algorithm introduced in AFDEX_V24R02. Figure 2.15(a) shows the configuration before analysis. In previous versions, interference issues occurred between materials in contact with the die, as illustrated in Figure 2.15(b). In AFDEX_V24R02, as shown in Figure 2.15(c), material penetration along the contact surfaces is effectively prevented, resulting in simulation results that are much closer to actual behavior.

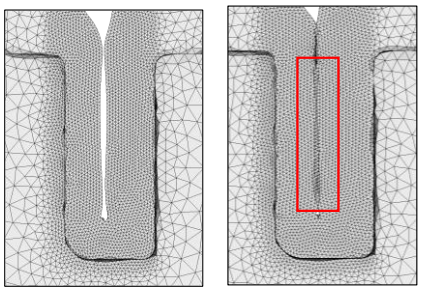

(a) Initial configuration (b) Previous prediction

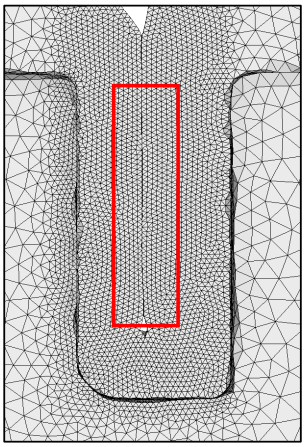

(c) Improved prediction

Figure 2.15 Continuous self-contact behavior between materials

3. Key User Interface Improvements

3.1 Extreme Mesh Generation for Dies

Figure 3.1(a) shows the die mesh for a single-die configuration, consisting of approximately 7.2 million tetrahedral elements. When a larger number of elements was specified, mesh generation failed due to memory limitations; however, a higher number of elements can be generated depending on the performance of the user's PC. Figure 3.1(b) presents a multi-die case composed of 10 die components, where each die component was discretized into 2 million tetrahedral elements.

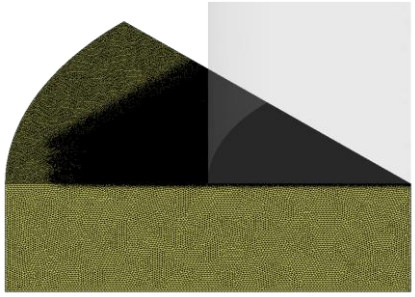

(a) Single die

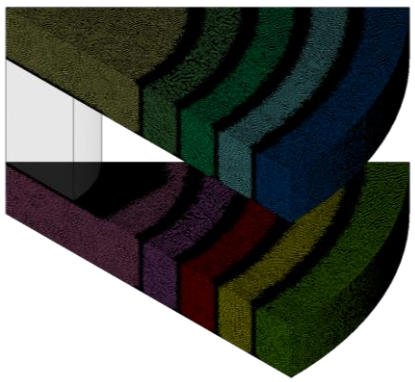

(b) Multiple dies

Figure 3.1 Verification of extreme mesh generation for dies

3.2 HDF5 Format Export

An export function supporting the HDF5 format has been added. This feature enhances interoperability by enabling simulation results to be efficiently linked with external tools. Figure 3.2 shows the HDF5 export dialog and the extracted result data.

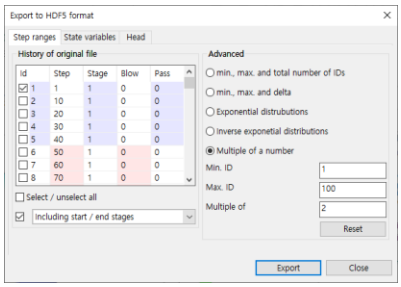

(a) HDF5 export dialog

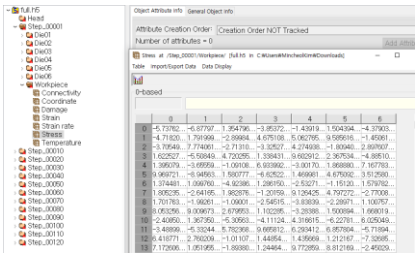

(b) Data opened in an HDF viewer

Figure 3.2 HDF5 export functionality

3.3 Forming Limit Curve (FLC) Input

In previous versions, Forming Limit Curve (FLC) data had to be defined during preprocessing in order to evaluate Forming Limit Diagram (FLD) results.

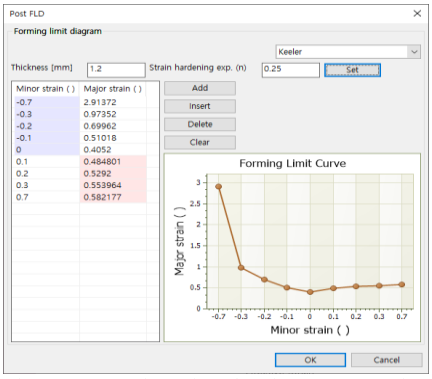

Figure 3.3 FLC input interface in post-processing

In the latest version, FLC data can be entered directly in the post-processing stage, eliminating the need to rerun simulations when FLC data are modified. Figure 3.3 shows the FLC input interface in the post-processor.

3.4 STL Model Overlay in Post-Processing

To support result verification and comparison, a function has been added that allows the predicted material shape to be overlaid with the original CAD model (STL). Figure 3.4 shows an application example at the final simulation step.

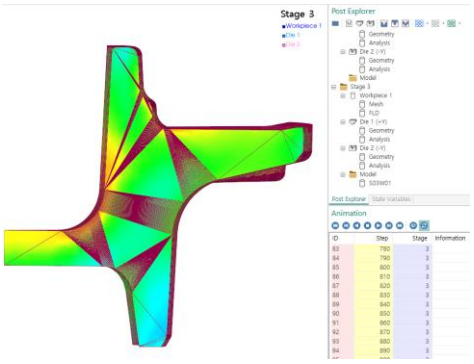

Figure 3.4 Comparison between STL model and simulation result at the final step

3.5 3D Piercing/Trimming UI

To reduce user errors during piercing or trimming setup, reference images have been added to the analysis condition input dialog, as shown in Figure 3.5. In addition, an issue in which simulations occasionally terminated without executing piercing or trimming operations has been resolved.

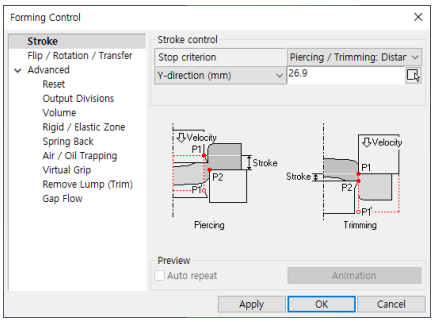

Figure 3.5 Piercing / trimming condition input dialog

3.6 Material-to-Material Friction for Single-Body Analysis

In previous versions, when material-to-material contact occurred in single-body analyses, friction conditions at the contact interface were internally assumed by the solver. Starting from AFDEX_V24R02, users can explicitly define material-to-material friction conditions not only for multi-body analyses but also for single-body analyses. Figure 3.6 shows the interface for specifying inter-object friction conditions and friction coefficients.

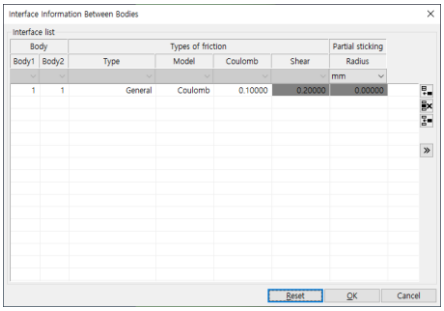

Figure 3.6 Material-to-material friction input dialog

3.7 Updated Default 2D Auto-Mesh Settings

AFDEX automatically configures analysis conditions to enhance usability. In the process information dialog, users can select Fast, Normal, or Accurate modes to balance computation speed and accuracy. Based on this selection, the number of elements and simulation steps are automatically determined. From AFDEX_V24R02, these default values have been increased by approximately 1.5 times compared to previous versions to improve solution accuracy.

3.8 Metal Flow Line Visualization

n previous versions, metal flow line visualization became inconvenient when the initial billet orientation was not aligned with the global x-, y-, or z-axes. In AFDEX_V24R02, an automatic center-axis detection function has been implemented. As a result, metal flow lines can now be visualized consistently regardless of the initial material orientation, as shown in Figure 3.7.

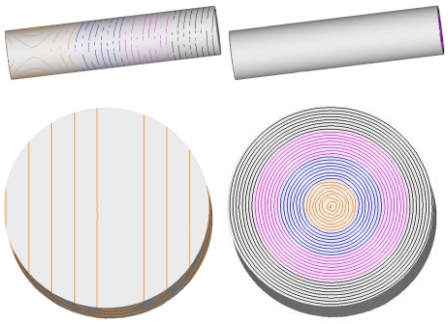

(a) Before improvement (b) After improvement

Figure 3.7 Improved metal flow line visualization

3.9 Heat Treatment Module GUI

Based on feedback collected during beta testing of the AFDEX heat treatment module, several usability improvements have been implemented in the preprocessing stage. For example, sample heat treatment processes are now provided when creating a new project, enhancing user convenience (Figure 3.8(a)). The heat treatment dialog allows users to visualize heat treatment cycles in chart form (Figure 3.8(b)). In the cycle dialog, users can define analysis steps, solver options, and heat transfer boundary conditions for each cycle (Figure 3.8(c)).

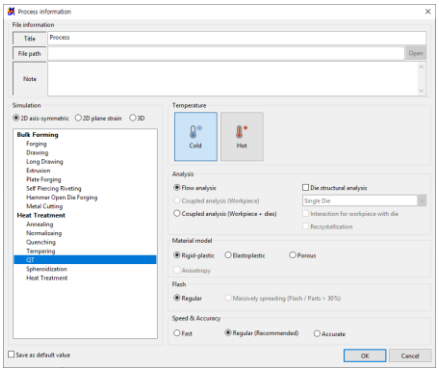

(a) Process control – sample heat treatment processes

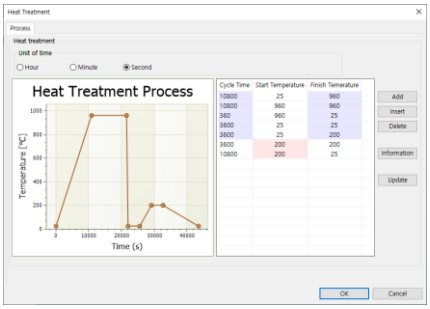

(b) Heat treatment setup dialog

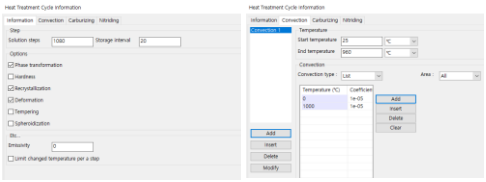

(c) Heat treatment cycle information dialog

Figure 3.8 Improved usability of the heat treatment module

3.10 2D DXF Import

In previous versions, shape recognition errors could occur when importing CAD data created using blocks. Starting from AFDEX_V26R01, models constructed with blocks can now be imported correctly. In addition, models created by inserting or copying and pasting blocks from other files are also fully supported.

3.11 Perspective Control in AFDEX_SP

Earlier versions provided only basic perspective adjustment. In response to user feedback, the latest version significantly improves usability and control of perspective settings. Figure 3.9 shows the perspective control dialog and application examples. This function allows users to apply realistic perspective effects when comparing photographs of forged products with simulation results, thereby enhancing visual realism and interpretability.

(a) Forged product

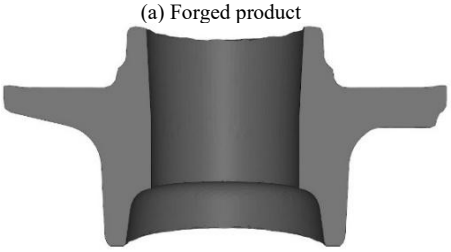

(b) Simulation result with perspective applied

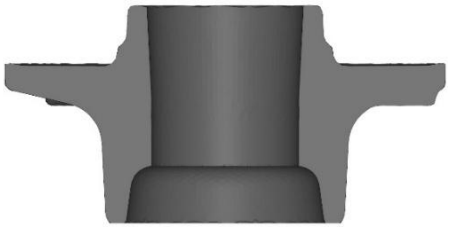

(c) Simulation result without perspective applied

Figure 3.9 Application example of perspective control

3.12 License Manager

From AFDEX_V24R01, the licensing system was transitioned to a network-based license. However, an issue existed where the license manager did not automatically start after rebooting the server PC. To resolve this, the license manager has been converted into a service application, and starting from AFDEX_V24R02, the server license manager has been separated from the client installation. As a result, the AFDEX license manager must be installed on the server PC, while client PCs can access licenses by entering the server IP address and port number.

4. Notices

4.1 Key Publications in 2025

1. S. H. Chung et al., 2025, Finite element analysis and experimental verification of the mechanical performance of a novel easy-to-splice mechanical coupler, Computers and Concrete, V. 35, pp. 127-136.
2. N. Y. Kim et al., 2025, Analytical and numerical evaluation of the relationship between elongation calibration function and cyber standard tensile tests for ductile materials, Materials and Design, V. 253, p. 113851.
3. A. A. Abd. Ghawi et al., 2025, Coupled elastoplastic FEM analysis of frictional boss forming, Next Research, V. 2, p. 100416.
4. H. M. Lee et al., 2025, Novel finite element analysis model for three-roller fillet rolling focusing on its strength of accuracy and practicability, Journal of Materials Research and Technology, V. 37, pp. 3788-3800.
5. M. K. Razali et al., 2025, Hot Extrusion Process Grain Size Prediction and Effects of Friction Models and Hydraulic Press Applications, Metals, V. 15, p. 887.
6. Y. Heo et al., 2025, Evaluation of an empirically evolved tube drawing process design based on the academic process design criteria, The International Journal of Advanced Manufacturing Technology, V. 140, pp. 5173-5187.
7. H. M. Lee et al., 2025, Experimental and numerical study on fillet rolling of a Ti6Al4V alloy aircraft bolt focusing on fatigue life, Journal of Manufacturing Processes, V. 151, pp. 490-505.
8. Y. Heo et al., 2025, Process optimal design of a tube drawing process in terms of residual stress homogeneity, Journal of Physics: Conference Series., V. 3144, p. 012018.
9. N. Y. Kim et al., 2025, An analytical model for correcting standard tensile test curves of different materials, Journal of Physics: Conference Series., V. 3144, p. 012019.
10. M. S. Joun et al., 2025, A Review of Friction and Lubricant in Metal Forming, Lubricants, V. 13, p. 512.
11. B. S. Hong et al., 2025, Combined elastoplastic finite element method and tube tensile test method to accurately characterize flow behaviors of tubular metallic materials, The International Journal of Advanced Manufacturing Technology, V. 141, pp. 5373-5388.
12. B. S. Hong et al., 2025, Determination of Damage Constant and Critical Damage by the Combined Experiment and FEM Using the Reference Processes, Metals, V. 15, p. 1376.

4.2 ICFG 58th Meeting

MFRC attended the 58th General Assembly of the International Cold Forging Group (ICFG) held in Valenciennes, France, from September 15 to 17, and officially became a member of this international forum.

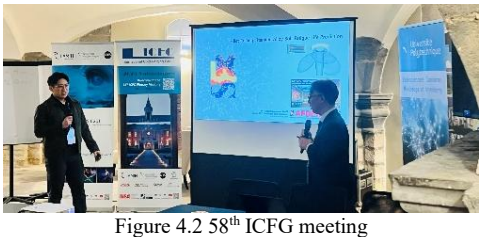

Figure 4.2 58th ICFG meeting

4.3 Workshops in Türkiye

MFRC, together with its Turkish partner Simultura Malzeme Teknolojileri, conducted a metal forming workshop in collaboration with the METAT team at Gazi University. In addition, MFRC held a heat treatment and microstructure workshop with the Metallurgy and Materials community at METU.

Figure 4.3 GAZI University workshop

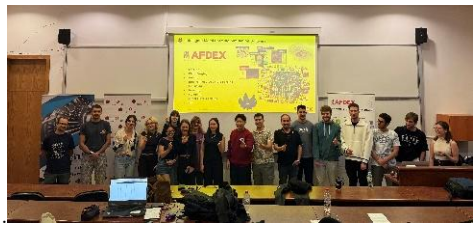

Figure 4.4 METU Workshop

4.4 Networking with Overseas Customers and Partners

Throughout 2025, MFRC has continuously strengthened collaboration with overseas partners and newly established customers. In particular, the company has actively expanded technical support activities to promptly resolve customer-specific technical issues and enhance the efficiency of AFDEX utilization. MFRC has also participated in several Altair AI+CAE technology events held across the APAC region, including Korea, Japan, Indonesia, Taiwan, and Malaysia.

(a) Altair Technology Day Indonesia 2025

(b) Altair Technology Conference Taiwan 2025

(c) Altair Technology Conference Japan 2025

(d) Altair Technology Conference Malaysia 2025

Figure 4.5 Altair AI+CAE Technology Events

4.5 MetalForm China 2025

MFRC participated in MetalForm China 2025, the largest metal forming exhibition in Asia, held in Shanghai, China, from June 17 to 20, 2025.

The AFDEX team received an Outstanding Exhibitor Award at the event.

4.6 Selected as a Korean Government–Designated Global Growth Company

In April 2025, MFRC was designated as a Korean government–recognized Global Growth Company under the Global Small Giant 1000+ program of the Ministry of SMEs and Startups. This recognition reflects strong evaluation of MFRC's proprietary CAE software development capabilities, continuous technological innovation, and high growth potential in global markets.

Through this designation, MFRC will receive government support for overseas expansion, research and development (R&D), and marketing activities, which will further strengthen its global competitiveness.

Going forward, MFRC will continue striving to deliver greater value to customers worldwide as a leading provider of metal forming process simulation solutions.